5 May 1978, Volume 200, Number 4341 **SCIENCE**

Sharpening Stellar Images

Real-time phase correction has permitted a ground-based telescope to overcome atmospheric distortion.

Andrew Buffington, Frank S. Crawford, Stephen M. Pollaine, Charles D. Orth, Richard A. Muller

If the Theory of making Telescopes could at length be fully brought into Practice, yet there would be certain Bounds beyond which Telescopes could not perform. For the Air through which we look upon the Stars, is in a perpetual Tremor; as may be seen by the tremulous Motion of Shadows cast from high Towers, and by the twinkling of the fix'd Stars. But these Stars do not twinkle when viewed through Telescopes which have large apertures. For the Rays of Light which pass through divers parts of the aperture, tremble each of them apart, and by means of their various and sometimes contrary Tremors, fall at one and the same time upon different points in the bottom of the Eye, and their trembling Motions are too quick and confused to be perceived severally. And all these illuminated Points constitute one broad lucid Point, composed of those many trembling Points confused and insensibly mixed with one another by very short and swift Tremors, and thereby cause the Star to appear broader than it is, and without any trembling of the whole. Long Telescopes may cause Objects to appear brighter and larger than short ones can do, but they cannot be so formed as to take away that confusion of the Rays which arises from the Tremors of the Atmosphere. The only Remedy is a most serene and quiet Air, such as may perhaps be found on the tops of the highest Mountains above the grosser Clouds.

—ISAAC NEWTON (*1*)

In the 250 years since these words were written, astronomers have been able to find neither a more succinct description of the "seeing" nor, until recently, a "Remedy" other than the one suggested by Newton. The speckled images of distant stars result directly from phase perturbations caused by propagation of the light through inhomogeneities in the atmosphere. The scintillation (intensity fluctuations) perceived by the eye as twinkling results from interference, which also develops as the perturbed wave propagates down through the atmosphere. However, the image quality is primarily degraded by the phase perturbations rather than the amplitude variations. A time exposure averages together the speckles, yielding a blurred image whose size depends on the observatory location and the particular turbulence at the time. At most observatory locations, however, this image size is seldom less than 1 second of arc. Thus, the resolving power of large telescopes is no better than that achieved by a mere 10-centimeter aperture; larger telescopes simply gather more light for observing dimmer objects.

A number of methods have been employed which partially overcome this seeing limitation. Interferometer techniques were introduced by Michelson and Pease (*2*). Intensity interferometry was invented and developed by Hanbury Brown (*3*) and R. Q. Twiss. Speckle interferometry was developed by Labeyrie and co-workers (*4*), and has recently yielded several newly separated binary star systems and refined the measurements on others (*5*). Knox and Thompson (*6*) suggested a method to extend speckle interferometry to nonsymmetrical objects. Their suggestion was successfully simulated at Itek Corporation (*7*) and used to reconstruct solar features (*8*). T. Brown (*9*) recently suggested a method which allows postdetection image retrieval through the use of nonredundant-array apodization of the telescope aperture. These techniques all require a narrow wavelength band-pass in recording the image, and the more powerful of them also require considerable computing for each image.

Babcock (*10*) first suggested a system which could provide real-time correction of astronomical images. He proposed that an active corrector plate be introduced into the telescope optics to compensate for the changing atmospheric phase shifts. To determine the amount of correction to apply to a particular region of the telescope objective, he suggested performing a knife-edge test on each portion of the objective, using an unresolved nearby bright star as the light source. Unfortunately, practical atmospheric time constants and spatial distributions require that this nearby star be quite bright and not very far removed in angle from the objects under study. Such nearby stars are rare, and Babcock's scheme has never been used. Another interesting scheme that would depend on use of a reference star is the phase-contrast method proposed by Dicke (*11*).

It now appears that real-time correction of astronomical telescope images is feasible, without the need for a nearby guide star (*12-14*). Several different schemes have been proposed to detect and correct the phase errors in the incident light wave, and a number of groups are now actively engaged in constructing and testing telescope systems which put these new ideas into practice

Andrew Buffington, Richard A. Muller, and Charles D. Orth are research physicists at the Lawrence Berkeley Laboratory and at the Space Sciences Laboratory, University of California, Berkeley 94720. Frank S. Crawford is a professor of physics at the University of California, Berkeley, and a research physicist at the Lawrence Berkeley Laboratory. Stephen M. Pollaine is a physics graduate student at the University of California, Berkeley.

0036-8075/78/0505-0489$01.00/0

(*15*). These schemes include the shearing interferometer (*12, 15*), the Hartmann interferometer (*15*), and the sharpness detector (*14–17*). This article describes the results we have achieved with a prototype one-dimensional system, using sharpness detection to determine the appropriate phase corrections.

Summary. Atmospherically induced phase perturbations have for years limited the resolution of large optical astronomical telescopes. A prototype telescope system with six movable elements has successfully corrected these phase perturbations. This use of real-time image sharpening has restored stellar images to the diffraction limit (in one dimension) for a 30-centimeter telescope. The double-star image presented indicates that the bulk of the atmospherically induced wave-front phase change occurred within 2 kilometers of the telescope. This implies that, at least for conditions similar to those of our measurement, real-time correction can be accomplished simultaneously for a region at least several arc seconds in angular size. With the present apparatus the technique should be practical for objects as dim as fifth magnitude, and with improvements the technique holds the promise of active image restoration for objects as dim as ninth magnitude.

Sharpness Detection

An image-plane sharpness, if defined suitably, has been shown to reach an absolute maximum only when the atmospheric phase perturbations have been removed. The sharpness measurement, then, is a suitable source of feedback to the active, phase-shifting elements of the corrector plate. We have shown that such feedback causes rapid convergence to the true restored image.

A wide variety of suitable sharpness functions are available. Computer simulations and formal proofs have been carried out for several of them (*14*). A selection of particularly useful functions is

$$S_1 = \int I^2(x,y)\, dx\, dy \tag{1}$$

$$S_2 = I(x_0,y_0), \text{ the intensity at a single image point } (x_0,y_0) \tag{2}$$

$$S_3 = \int I(x,y)\, M(x,y)\, dx\, dy \tag{3}$$

$$S_4 = \int \left| \frac{\partial^{n+m} I(x,y)}{\partial x^n \partial y^m} \right|^2 dx\, dy \tag{4}$$

$$S_5 = \int I^n(x,y)\, dx\, dy,\ n > 1 \tag{5}$$

where (x,y) are image-plane coordinates, $I(x,y)$ denotes image-plane intensity, and $M(x,y)$ is a mask which approximates the true restored image. In choosing an appropriate sharpness function for practical applications, one must consider both the ease with which the sharpness can be measured and the type of object to be studied. For the simple case of a single unresolved star, perhaps with dim companions or structure nearby, or an object with a single bright "glint" on it, S_2 would probably be the best choice, since a single photomultiplier provides the measurements when placed behind an image-plane mask pierced by a hole the size of a diffraction-limited image. For a complicated object such as a tumbling asteroid or satellite, S_1 would probably be optimum, although its use might require some difficult image-plane data processing. To view a planet, one would probably use a function of the type S_4, in which the sharpness of the edge of the planet drives the feedback. The rings of Saturn might be best recorded with a variant of S_3, however. One would use the best available Saturn photograph to generate a starting $M(x,y)$, but then update the mask with newly sharpened images as they are recorded. These sharpness functions are successful because they single out some feature of the object which is known to be a maximum with the undistorted image, and use the amount of the feature present to provide a measure of the distortion.

Apparatus

In this section we give a brief description of the design, calibration, and test of our apparatus; details have been published elsewhere (*17*). Figure 1 shows a schematic diagram of the image-sharpening system, and Fig. 2 shows the mechanical layout of the apparatus. This first telescope was designed to be as simple as possible, yet have a resolution fine enough to be capable of interesting astronomical measurements, such as the separation of double stars. It has a 32-cm-diameter primary mirror with an entrance aperture measuring 30 by 5 cm. This aperture can be thought of as consisting of six separately adjustable squares. (The phase adjustment actually occurs at the second diagonal mirror, described below.) The primary mirror, which has a 2.5-meter focal length, focuses the incident light immediately in front of the projection lens. The light path is folded by two diagonal mirrors on its way to the primary image. The first diagonal mirror is mounted on three piezoelectric columns which allow steering of the image. The second diagonal mirror consists of six independently movable elements which can change the optical pathlength of light passing through the six entrance-aperture squares by ±2.5 micrometers. The projection lens makes an enlarged image on a slit in front of the sharpness-defining photomultiplier PM-1, which measures sharpness of the type S_2. A bimetal strip system automatically keeps this projection lens properly focused as temperature changes occur. A portion of the light is diverted to the image-recording photomultiplier PM-2. The image is moved across the slit of PM-2 either by mechanically translating the PM-2 assembly or by displacing the image by transmission through a rotating glass cube (not shown in Fig. 2) placed between the beam splitter and the PM-2 slit. The balance of the light not passing through the slit of PM-1 is detected by photomultipliers PM-3 and PM-4 and is used to drive the first diagonal mirror at rates $\leqslant 50$ hertz to keep the image centered on the sharpness-defining slit.

The 30 by 5 cm aperture, when corrected, has six times better resolution in one direction than the other. Rather than attempt to utilize the image information in the direction of poorer resolution, we have integrated over this direction by using slits both to define the sharpness and to record the image. Since we expect to use this instrument primarily for objects which consist of a few unresolvable bright points, the one-dimensionality of the recorded images is not detrimental. Our computer simulations (*14*) have shown that no fundamental difficulty stands in the way of making two-dimensional image-sharpening systems; the choice of one-dimensional imaging for this apparatus came primarily from the desire to keep the design simple.

The measurement of S_2 is given by the current from PM-1. This provides the feedback to drive the independently movable elements making up the second diagonal mirror. The six elements move as pistons perpendicular to their common plane. How this "flexible mirror" is made and the alignment procedures which guarantee coplanarity of the six elements have been described previously (*17*). The electronics providing the feedback link between PM-1 and the movable mirrors is shown schematically in Fig. 3, along with the steering and data-recording systems. The program logic causes the mirror logic to introduce a small perturbation (typically 0.05 to 0.10 μm) into the position of one of the six movable mirrors. The comparator determines whether this perturbation increased the sharpness reading in PM-1. If it did, the perturbation is left in place; otherwise it is removed. The circuits cycle through each of the six mirrors in turn, continually building up the value of S_2 through successful introduction of perturbations. Opposite signs of perturbation are used on successive passes through the mirrors, to prevent the adjustments from eventually working the mirror motions to the extremes of their ranges.

The length of time the system takes to pass through a complete cycle of six mirror adjustments depends on the integration time chosen for the comparator to decide whether to replace a perturbed mirror. The integration time can be less than 0.1 millisecond for many of the brightest stars in the sky, but has to be several milliseconds for a typical fifth-magnitude star, in order that photoelectron statistical fluctuations not confuse the decisions. The cycle time can be varied from a minimum of about 1 msec (the time it takes to perturb six mirrors and replace on the average half of them) to about 30 msec, depending on the integration time selected. It takes about three cycles through the mirrors to produce an adequately sharpened image.

The apparatus was first tested with laser light viewed horizontally along a 250-m path. Figure 4 shows the result on a day when the atmosphere had spread the image to about 3 arc sec, but the speckle change time was quite long. The recorded and expected images are in good agreement. The wings of the diffraction pattern are due in about equal part to the expected pattern in the absence of any atmospheric perturbation and to the errors that remain because the incident phase front was corrected by six discontinuous pistons rather than a smoothly deformable mirror. The series of bumps on either side of the main diffraction peak, at multiples of 2.6 arc sec, are caused by the regularly spaced gaps between the six movable mirrors.

The rapidity of the speckle changes at the sharpness slit determines the dimmest object that can be corrected by this system. A measure of the speckle change time is given by

$$A(\tau) = \int_0^T dt\, I(t) \cdot I(t + \tau)$$

where $I(t)$ is the current from PM-1 with feedback off. The integral is performed by a Hewlett-Packard Correlator, model 3721A, with $T >> \tau$ and $A(0)$ normalized to unity. We define the characteristic coherence time τ_c to be the value for which $A(\tau)$ has dropped to half of $A(0)$. For the horizontal-path tests, τ_c varied from several to nearly 100 msec. Since $A(\tau)$ gives the time structure for speckles drifting

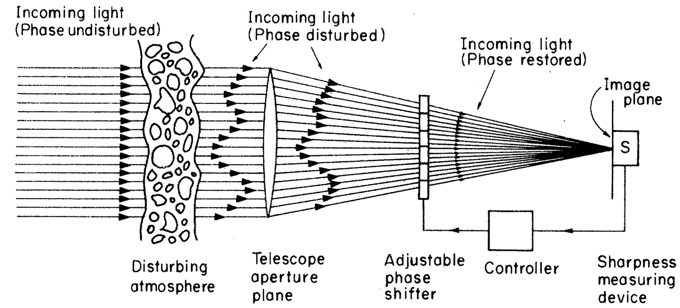

Fig. 1. Schematic diagram of the image-sharpening system. Arrowheads indicate the relative phase of the wave. The adjustable phase shifter corrects the phase of the incoming wave. [From Muller and Buffington (*14*)]

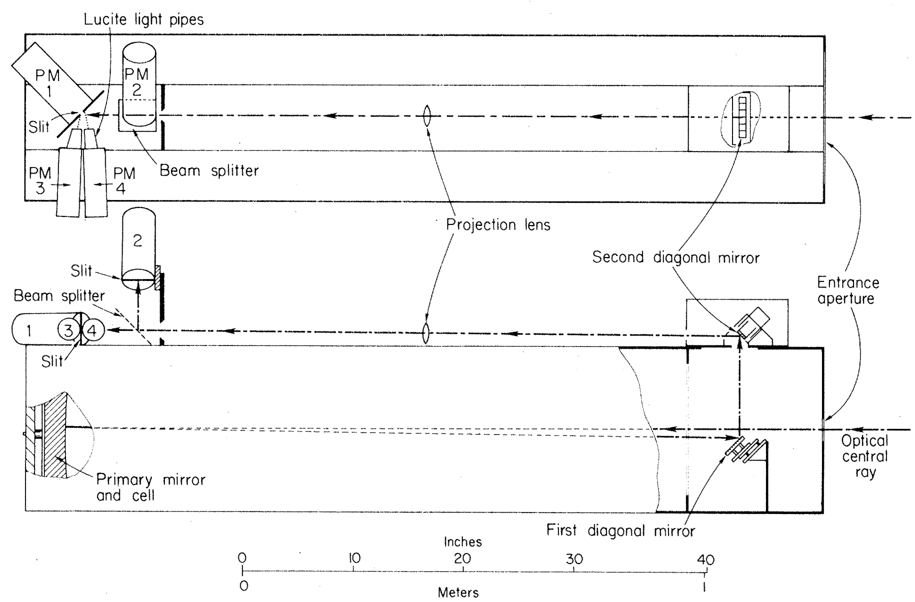

Fig. 2. Mechanical layout of the apparatus. The telescope mount (not shown) allows rotation of the entire telescope about the axis of its barrel, thus permitting orientation of the direction of good resolution. [From Buffington *et al.* (*17*)]

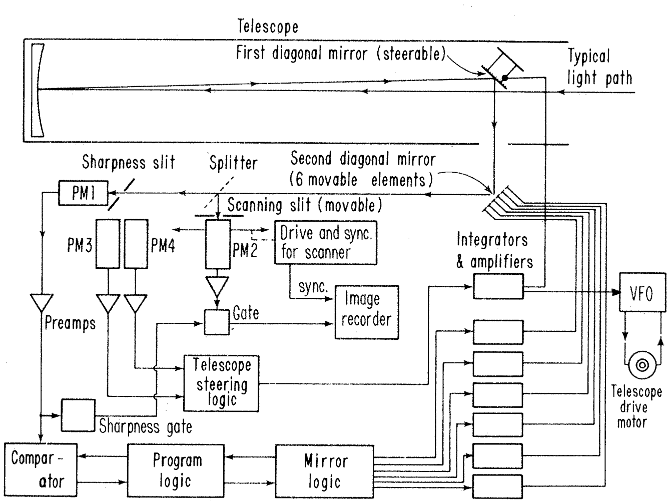

Fig. 3. Block diagram of the electronics. The incident light reflects off the first and second diagonal mirrors and then proceeds to the four photomultipliers. PM-1 is used to define the image sharpness and provide feedback to the six movable elements of the second diagonal mirror; PM-2 receives a portion of the light to record the image; and PM-3 and PM-4 receive the light not passing through the sharpness slit and drive the first diagonal mirror to keep the image centered on the sharpness slit. When viewing stars, the average steering correction is fed to the telescope mount drive motor, which then corrects the speed of the drive to keep the first diagonal steering centered within its range. This permits the use of a crude spur-gear telescope drive, but nonetheless provides stellar tracking at better than 1 arc sec. The image is scanned over the PM-2 slit by a rotating cube, which also provides synchronization signals for the image-recording system. Image recording is permitted only when the sharpness signal from PM-1 exceeds a preset value.

and changing at the sharpness slit, τ_c is an indication of how rapidly the phase adjustments must be completed in order to achieve a corrected image. We have found empirically, for perturbations of 1/5 to 1/10 wavelength, that the system must be able to complete about three cycles through the six mirrors within τ_c in order to achieve a well-corrected image. Thus the measurement of a particular τ_c at some observing location and time determines the maximum permissible length of the electronics cycle time, and hence the longest permissible sharpness integration time. This integration time in turn determines the dimmest correctable object, which is limited by photon statistics. The integration adjustment for our instrument, from 10 μsec to 4 msec, matches the shortest possible integration time for the brightest star in the sky and the longest coherence time (50 to 100 msec) we thought might ever be encountered at observatories. We used this instrument to measure τ_c at our laboratory site in Berkeley, at nearby Leuschner Observatory, at Lick Observatory on Mount Hamilton, and at Hale Observatory on Mount Wilson. Figure 5 shows the distributions.

Since seeing conditions frequently vary with time, we found it important to gate the image-recording system, using the sharpness signal from PM-1. The gate circuit permits recording the image only when the measured sharpness in PM-1 exceeds a preset value. Thus when τ_c suddenly deteriorates to a small value and then slowly recovers, the data recording is switched off until the image-sharpening system is again able to "keep up" with the speckle changes, as indicated by a return to large signals detected in PM-1.

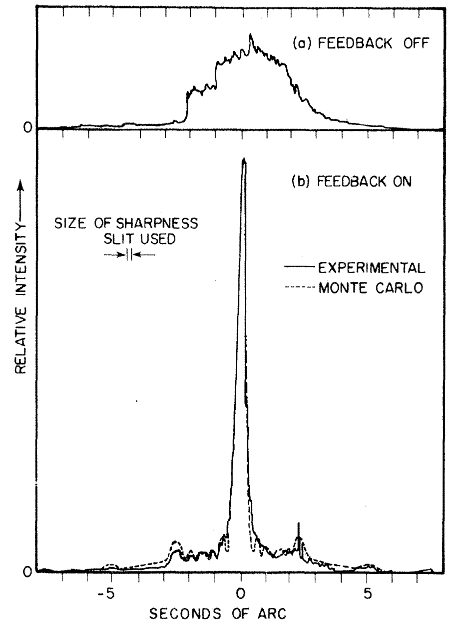

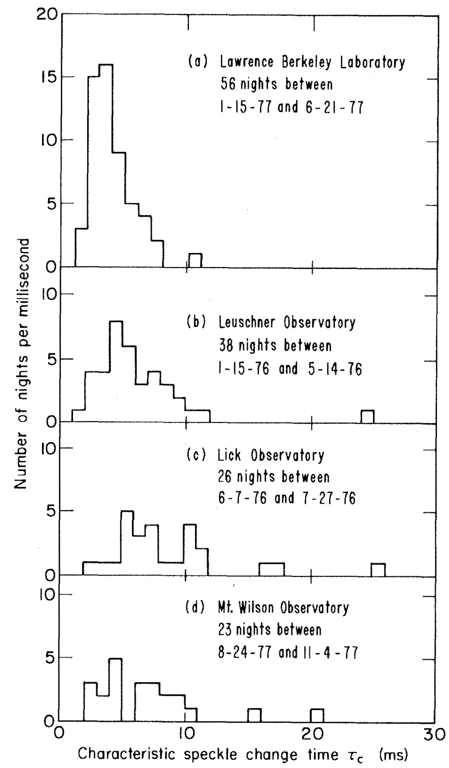

Fig. 4 (left). Images of laser light viewed horizontally along 250 m of turbulent atmosphere. [From Buffington *et al.* (*17*)] Fig. 5 (right). Characteristic speckle change times at four observatory locations. All measurements during one night have been averaged together. The data shown may be misleading because there are seasonal variations in the seeing, and the data for the observations were collected at different times of the year. Furthermore, the histogram represents only the average seeing for the night. At Mount Wilson, in particular, there were nights when τ_c was greater than 15 msec for a substantial portion of the time, but the whole night still averaged less than 10 msec.

Sharpening Stellar Images

The apparatus has been operated attached to other telescopes at Leuschner and Lick Observatories, and with its own equatorial mount at the Lawrence Berkeley Laboratory and at Mount Wilson Observatory. Some of the earlier results have already been reported (*18*). Figure 6 shows the first sharpened stellar image obtained with this apparatus. The image-recording gate was not available when this image was taken; based on subsequent experience with the gate, it would have reduced the underlying background in Fig. 6b. The peak riding on the background is nearly diffraction-limited for a telescope of this size. To our knowledge, this was the first time that real-time correction of atmospheric seeing succeeded in producing a diffraction-limited stellar image.

Figure 7 shows other images, taken more recently at Mount Wilson Observatory, with the gate operational and using the rotating cube system for image recording. It demonstrates the ability of the gate to reduce the background of the

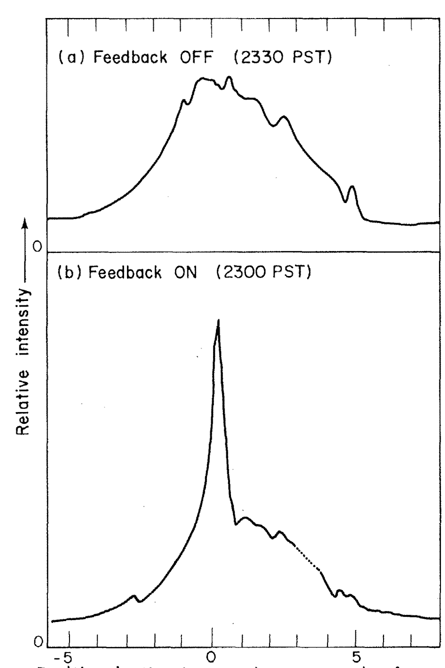

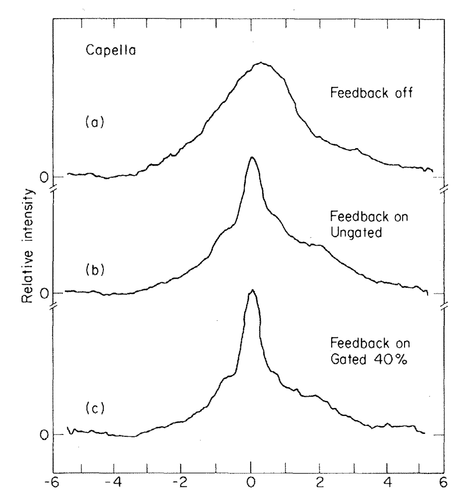

Fig. 6 (left). Images of Sirius recorded at Leuschner Observatory on the evening of 21 January 1976 (*P.S.T.*, Pacific standard time). [From Buffington *et al.* (*18*)] Fig. 7 (right). Images of Capella recorded at Mount Wilson on 3 November 1977. The gating fraction in (c) was the best 40 percent. For these images τ_c was about 13 msec. Since two of the movable elements were inoperative for the images shown here and in Fig. 8, the images are for a telescope with an aperture size of 5 by 20 cm and only four movable elements. The peaks are still close to the diffraction limit for this smaller aperture.

ungated curve, although the background was less severe in this case than it was on the image in Fig. 6b. One might wonder whether the gate alone could allow recording of an image as good as that of Fig. 7c, without the image sharpening provided by the movable mirrors. In principle this might be the case, since the gate could detect those moments when the seeing permitted a diffraction-limited image and placed it on the PM-1 slit. However, when we tried using the gate alone, the resulting images were substantially broader than those achieved with the full image sharpening in operation. A gate-only system might be successful, however, if the seeing were such that it primarily moved the image from side to side rather than disrupting it into speckles.

Figure 8 shows images of a double star. The brighter of the two stars (the one on the left) was placed on the sharpness-defining slit, and the steering circuit was biased to keep the image centered that way. It is clear that the pair of stars is much better resolved by this system than it could have been without image sharpening. Figure 8 also shows that most of the seeing perturbations at Mount Wilson on that night did not originate high in the atmosphere, since the image of the dimmer star is at most 20 percent wider than that of the brighter star, whose sharpness was maximized. Had all of the phase perturbations originated farther than 5 km from the telescope, we would expect the second peak to be completely degraded relative to the first because light from the two different stars would then have passed through different atmosphere on its way to each of the segments of the telescope mirror. Our analysis of the shapes of the two peaks indicates that the bulk of the phase perturbations originated within 2 km of the telescope.

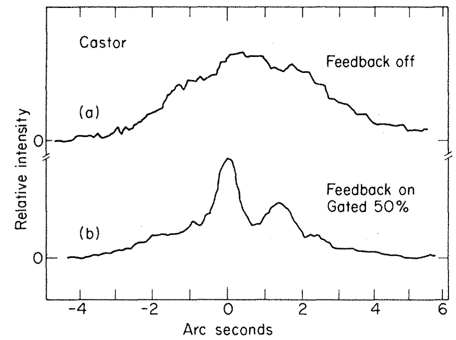

Fig. 8. Images of Castor recorded at Mount Wilson on 3 October 1977. The gating fraction in (b) was the best 50 percent. The direction of good resolution of the telescope was oriented about 50° from the line between the two stars, so the two peaks appear somewhat closer to each other than their actual 2 arc sec separation. For these images τ_c was about 20 msec.

Discussion

The apparatus described in this article was matched for seeing with a characteristic angular size of several arc seconds. For uncorrected images of this size and somewhat larger, we have shown that dramatic improvement results when image sharpening is applied. Such improvement promises better resolving power at existing observatories, allowing both the discernment of finer details and the use of narrower slits in spectrometers without loss of light. For multiple star systems, this would allow separate spectral measurements with the individual stars. If the seeing is much worse than several arc seconds, diffraction-limited performance is no longer achieved and a large uncorrected background results, rather like that in the ungated images shown in Figs. 6b and 7b. Gating cannot remove this background since it is caused by phase changes in the incident wave front of much more than 1 radian within a single movable mirror. The acceptable size of seeing disk that a particular system can correct depends on the type of measurement one wants to perform; for a close (but still resolvable) pair of stars with comparable intensities, the presence of the two peaks can still be seen above the background. On the other hand, for resolving a dim companion star, one may require that the uncorrected background be minimized. In some cases the companion star may be so dim that even absence of any seeing distortion (attainment of the unperturbed diffraction pattern) might not allow resolution, and the presence of the faint star would then have to be inferred through other means.

The telescope simultaneously corrects all light wavelengths, which is vital for spectroscopic applications. In cases that require maximizing the light through a narrow slit, large tails on the diffraction pattern may not matter at all. Then, use of image sharpening improves the photon flux through the slit as the seeing worsens, until the transverse distance for 1 radian of phase change becomes significantly smaller than the size of one of the movable mirrors. For seeing worse than this, diffraction-limited performance is no longer possible, and the amount of light in the central peak diminishes inversely as the diameter of the seeing disk. However, image sharpening can still provide an image whose peak intensity is roughly N times that of the background, where N is the number of mirror segments.

The intensity of the dimmest object correctable in real time is inversely proportional to the speckle change time. The apparatus described here should correct objects down to fifth magnitude for a τ_c of 30 msec. If the photon efficiency of the apparatus were maximized we could reach seventh magnitude.

In going to a larger telescope we would probably use a larger number of mirror segments. For example, using 10 by 10 cm segments, a filled one-dimensional array of length 2.5 m would have N = 25. A corresponding two-dimensional array in the form of an annular ring would have N = 75. However, a "nonredundant" linear array 2.5 m in length could have as few as N = 7. With our present instrument, which moves mirrors one at a time, the least permissible brightness of a correctable object is proportional to N^2 (14). This limitation occurs because both the sharpness change produced by moving a single mirror and the time available to do it diminish in proportion to $1/N$. Other strategies can move $N/2$ mirrors at a time, and these give a least permissible brightness proportional to N. An additional advantage might be obtained if the mirror movement functions were matched to the spectrum of atmospheric fluctuations. For our present small telescope with N = 6 there would be little or no advantage (theoretically or experimentally) in adopting these strategies. For larger N, however, the advantage would be substantial. We believe that a significant improvement in the resolution of large telescopes is possible for objects as dim as ninth magnitude, using sharpness detection. Other techniques (for example, a shearing interferometer or multi-image telescope) may do as well, but we do not believe that they can do significantly better.

Many interesting astronomical objects are brighter than this. For example, it should be possible to increase further the number of visually separated binary-star systems. One such system is μ Cassiopeia, which is of interest in connection with determining the primordial helium abundance (19). An adaptation of the techniques described here to a somewhat larger telescope aperture (say 1 m) should permit observation of μ Cassiopeia's dim companion, even if the magnitude difference is as great as ~ 5. Increased telescope angular resolution should also extend substantially the sample of stars whose masses can be determined because they are members of visually separated binary systems.

References and Notes

1. I. Newton, *Opticks*, Book I, Part I, Proposition VIII, Problem II (1730) (Dover, New York, 1952).
2. A. A. Michelson and F. G. Pease, *Astrophys. J.* **53**, 249 (1921).
3. R. Hanbury Brown, *The Intensity Interferometer* (Halsted, London, 1974).
4. A. Labeyrie, *Astron. Astrophys.* **6**, 85 (1970); D. V. Gezari, A. Labeyrie, R. V. Stachnik, *Astrophys. J.* **173**, L1 (1972).
5. H. A. McAlister, *Astrophys. J.* **215**, 159 (1977).
6. K. T. Knox and B. J. Thompson, *ibid.* **193**, L45 (1974).
7. P. Nisenson, D. C. Ehn, R. V. Stachnik, *Proc. Soc. Photo-Opt. Instrum. Eng.* **75**, 83 (1976).
8. R. V. Stachnik, P. Nisenson, D. C. Ehn, R. H. Hudgin, V. E. Schirf, *Nature (London)* **266**, 149 (1977).
9. T. M. Brown, *J. Opt. Soc. Am.*, in press.
10. H. W. Babcock, *Publ. Astron. Soc. Pac.* **65**, 229 (1953); *J. Opt. Soc. Am.* **48**, 500 (1958).
11. R. H. Dicke, *Astrophys. J.* **198**, 605 (1975).
12. J. W. Hardy, J. Feinlieb, J. C. Wyant, in "Digests of Technical Papers for the Topical Meeting on Optical Propagation through Turbulence," 9 to 11 July 1974, Boulder, Colo., paper TH-B1; J. W. Hardy, J. E. Lefebvre, C. L. Koliopoulos, *J. Opt. Soc. Am.* **67**, 360 (1977).
13. T. R. O'Meara, U.S. Patent No. 3,975,629 (1976).
14. R. A. Muller and A. Buffington, *J. Opt. Soc. Am.* **64**, 1200 (1974).
15. For partial descriptions of these systems see "Digests of Technical Papers for the Topical Meeting on Optical Propagation through Turbulence," 9 to 11 July 1974, in Boulder, Colo.; "Digests of Technical Papers for the Topical Meeting on Imaging in Astronomy," 18 to 21 June 1975, Cambridge, Mass.; "Imaging through the atmosphere," *Proc. Soc. Photo-Opt. Instrum. Eng.* **75** (1976); *J. Opt. Soc. Am.* **67** (No. 3) (1977).
16. S. L. McCall, T. R. Brown, A. Passner, *Astrophys. J.* **211**, 463 (1977).
17. A. Buffington, F. S. Crawford, R. A. Muller, A. J. Schwemin, R. G. Smits, *J. Opt. Soc. Am.* **67**, 298 (1977).
18. A. Buffington, F. S. Crawford, R. A. Muller, C. D. Orth, *ibid.*, p. 304.
19. For example, see J. Faulkner, *Phys. Rev. Lett.* **27**, 206 (1971).

20. A. J. Schwemin and R. G. Smits contributed much to the design and construction of the apparatus. The observatory measurements would have been impossible without the enthusiastic support of the staff of the Astronomy Department at Berkeley, the Lick Observatory staff, and the Mount Wilson Observatory staff. We are pleased with the continuing interest and support of L. W. Alvarez, H. W. Babcock, R. W. Birge, P. B. Boyce, and D. E. Osterbrock. D. D. Cudaback made several important contributions. We have enjoyed interesting conversations with L. V. Kuhi, J. E. Nelson, J. A. Tyson, G. Wallerstein, and E. J. Wampler. This work was supported by the Department of Energy and by grants from the National Science Foundation and the National Aeronautics and Space Administration.

The Genome of Simian Virus 40

V. B. Reddy, B. Thimmappaya, R. Dhar, K. N. Subramanian, B. S. Zain, J. Pan, P. K. Ghosh, M. L. Celma, S. M. Weissman

Summary. The nucleotide sequence of SV40 DNA was determined, and the sequence was correlated with known genes of the virus and with the structure of viral messenger RNA's. There is a limited overlap of the coding regions for structural proteins and a complex pattern of leader sequences at the 5′ end of late messenger RNA. The sequence of the early region is consistent with recent proposals that the large early polypeptide of SV40 is encoded in noncontiguous segments of DNA.

Simian virus 40 (SV40) is a small virus that replicates in the nucleus of host cells and may also transform cells from a variety of species (*1*). During the lytic cycle, gene expression is temporally regulated. Prior to viral DNA replication, one-half of one strand of the genome (the early region) is transcribed, forming cytoplasmic polyadenylated messenger RNA (mRNA). This mRNA, which is termed early RNA, is also present in most cells transformed by SV40 and directs the synthesis of this early mRNA. After the initiation of viral replication, the other strand of the other half of the DNA (the late region) is transcribed into mRNA (referred to here as late mRNA) that directs the synthesis of viral structural proteins. This virus has been the subject of intensive investigation as a model system for genes functioning in the nuclei of animal cells and for viral transformation of cells in culture. The genome of the virus consists of a circular DNA molecule containing more than 5200 base pairs (bp). In spite of the limited information in this DNA, the virus has a complex genetic structure and exhibits features of gene organization and expression different from those so far detected in prokaryotes.

In one approach to the detailed understanding of virus function, Fiers and his colleagues and our laboratory have separately determined the nucleotide sequence of the viral DNA. In this article, we present some of the principal features of this sequence (Fig. 1). More detailed reports of portions of the sequence have been published or are still in preparation (*2–14*).

This article represents work done by the authors while members of the Department of Human Genetics or the Department of Medicine (or both), at the Yale University School of Medicine, New Haven, Connecticut 06510. The present address of B. Thimmappaya is University of Connecticut Medical School, Farmington 02100; that of R. Dhar is National Institutes of Health, Bethesda, Maryland 20014; that of R. N. Subramanian is the Microbiology Department, University of Illinois Medical School, Chicago 60680; that of B. S. Zain is Cold Spring Harbor Laboratory, Cold Spring Harbor, New York 11724; that of M. L. Celma is Departmento de Microbiologia, Centro Ramon y Cajal, Carretera de Colmenar, Room 9.1, Madrid 34, Spain.

Regions Know to Code for Identified Viral Proteins

SV40 virus codes for at least four proteins. The major viral structural protein, VP1, has a molecular weight, estimated by sodium dodecyl sulfate gel electrophoresis, of 43,500 to 48,000 (*15*). The virus also codes for two minor structural proteins, VP2 and VP3, whose estimated molecular weights are 39,000 and 27,000 (*15*), respectively, and one large "early" protein (the A protein or T antigen) (*16–18*), which is necessary for initiation of rounds of DNA replication and for cell transformation. The molecular weight of the A protein has been estimated by sodium dodecyl sulfate gel electrophoresis as approximately 94,000.

There are three stretches of DNA in the SV40 genome whose RNA transcripts contain an AUG base triplet (A, adenylic acid; U, uridylic acid; G, guanylic acid) followed by a long run of sense codons (Fig. 2). The first of these begins at residue 1423 of Fig. 1. The initial sequences of this region were determined by Fiers *et al.* (*12*) and found to agree fully with the amino acid sequence of the amino terminus of VP1. Proceeding from the AUG at position 1423 (Fig. 1), there are 361 subsequent sense codons in phase, followed by a single UGA termination codon. This sequence predicts that the carboxyl-terminal amino acid of VP1 is glutamine; and this prediction has been confirmed experimentally (*19*). The predicted amino acid composition for VP1 is in good agreement with the experimental values (*20*). Some tryptic peptides of VP1 have been

0036-8075/78/0505-0494$02.00/0